

## Nature of Quiet Sun Oscillations Using Data from the *Hinode*, TRACE, and SOHO Spacecraft

G. R. Gupta<sup>1,2,3</sup> · S. Subramanian<sup>4</sup> · D. Banerjee<sup>1</sup> ·  
M. S. Madjarska<sup>4</sup> · J. G. Doyle<sup>4</sup>

© Springer ●●●

### Abstract

We study the nature of quiet-Sun oscillations using multi-wavelength observations from TRACE, *Hinode*, and SOHO. The aim is to investigate the existence of propagating waves in the solar chromosphere and the transition region via analyzing the statistical distribution of power in different locations, *e.g.* in bright magnetic (network), bright non-magnetic and dark non-magnetic (inter-network) regions, separately. We use Fourier power and phase-difference techniques combined with a wavelet analysis. Two-dimensional Fourier power maps were constructed in the period bands 2–4 minutes, 4–6 minutes, 6–15 minutes, and beyond 15 minutes. We detect the presence of long-period oscillations with periods between 15 and 30 minutes in bright magnetic regions. These oscillations were detected from the chromosphere to the transition region. The Fourier power maps show that short-period powers are mainly concentrated in dark regions whereas long-period powers are concentrated in bright magnetic regions. This is the first report of long-period waves in quiet-Sun network regions. We suggest that the observed propagating oscillations are due to magnetoacoustic waves which can be important for the heating of the solar atmosphere.

**Keywords:** Chromosphere, Quiet; Transition Region; Oscillations; MHD waves

### 1. Introduction

Although oscillations in the solar photosphere and chromosphere were first detected in the 1960s, they are not as yet well understood as in the photosphere. When the solar atmosphere is observed at chromospheric heights (Ca II H and K lines), a bright web-like cellular pattern called “the chromospheric network” pattern is clearly distinguishable (Hale and Ellerman, 1904). This Ca II network pattern overlies the photospheric magnetic-field concentrations clustered in the supergranular down-flow lanes (Simon and Leighton, 1964; Skumanich, Smythe, and Frazier, 1975). Regions outside the network pattern are called

---

<sup>1</sup>Indian Institute of Astrophysics, Koramangala, Bangalore 560 034, India. email: girjesh@gmail.com

<sup>2</sup>Joint Astronomy Programme, Indian Institute of Science, Bangalore 560 012, India.

<sup>3</sup>Presently at Max Planck Institute for Solar System Research, 37191, Katlenburg-Lindau, Germany.

<sup>4</sup>Armagh Observatory, College Hill, BT61 9DG, Armagh, N. Ireland.

the inter-network. The distinct properties of these network and inter-network regions are subject to intense studies (Hasan, 2008).

At the chromospheric level, five and three-minute oscillations were found to be associated with the network and inter-network regions (Dame, Gouttebroze, and Malherbe, 1984). Lites, Rutten, and Kalkofen (1993) showed that, only the three-minute inter-network oscillations are well correlated with the oscillations in the underlying photosphere, unlike the long-period 5–20 minutes network oscillations, which were not correlated with the photospheric disturbances. Carlsson, Judge, and Wilhelm (1997) observed phase-differences between the continuum and chromospheric line intensities and interpreted them as a manifestation of upward-propagating waves. Similarly, Wikstøl *et al.* (2000) also observed upward-propagating waves in the upper chromosphere which drove oscillations in the transition region, thus extending the evidence for the upward-propagating waves from the photosphere up to the base of the corona. Judge, Tarbell, and Wilhelm (2001) suggested that the chromospheric oscillations are primarily in response to the  $p$ -mode oscillations and are often strongly influenced by the photospheric magnetic fields before they could reach the transition region. Recently, Vecchio *et al.* (2007) proposed that a large fraction of the chromospheric acoustic power at frequencies below the acoustic cut-off, residing in the proximity of the network field elements, can directly propagate from the underlying photosphere. These results show that network magnetic elements can channel low-frequency photospheric oscillations into the chromosphere, thus providing a way to input mechanical energy into the upper atmosphere (De Pontieu, Erdélyi, and James, 2004; Jefferies *et al.*, 2006).

Areas surrounding the quiet-Sun network elements which lack oscillatory power in the 2–3 minutes range are termed as “magnetic shadows” (Judge, Tarbell, and Wilhelm, 2001; McIntosh and Judge, 2001). Vecchio *et al.* (2007) showed that a large fraction of the quiet chromosphere, surrounding the network regions, is occupied by such magnetic shadows which originate from the fibril-like structures observed in the core intensity of the Ca II line. While studying the magnetic network at the boundary of an equatorial coronal hole using data from TRACE 1600 Å and 171 Å passbands, Tian and Xia (2008) found a lack of power at high frequencies (5.0–8.3 mHz) and significant power enhancements at low (1.3–2.0 mHz) and intermediate frequencies (2.6–4.0 mHz) above the magnetic network. Recently, Kontogiannis, Tsiropoula, and Tziotziou (2010) found three and five minutes power enhancements around the network, forming power halos at photospheric heights. These power halos were replaced by magnetic shadows at chromospheric heights, indicating the existence of both upward and downward propagating waves.

In this work, we investigated the wave properties from a statistical point of view using *Hinode*/SOT, SOHO/MDI, and TRACE data. Our focus was mainly on the distribution of Fourier power over the quiet Sun, particularly the low-frequency domain. We also investigated the influence of small scale network magnetic fields on wave properties. For this, we analyzed the power and phase-difference between oscillations observed simultaneously in the chromosphere and the low transition region in bright magnetic regions (network), bright non-magnetic regions, and dark non-magnetic (inter-network) regions of the quiet Sun.

## 2. Observations and Data Reduction

Simultaneous observations obtained near disk centre on 9 April 2007 with the *Solar Optical Telescope* (SOT; Tsuneta *et al.*, 2008) onboard *Hinode*, with the *Transition Region and*

**Table 1.** Description of the observation.

	SOT	TRACE	MDI
<b>Time (UT)</b>	11:50–16:59	11:50–16:59	12:00–15:19
<b>Bandpass/Wavelength (Å)</b>	Ca II H	1550 filter	Ni I 6768
<b>FOV</b>	112" × 56"	384" × 384"	600" × 600"
<b>cadence (seconds)</b>	30	35	60

*Coronal Explorer* (TRACE; Handy *et al.*, 1999), and *Michelson Doppler Imager* (MDI; Scherrer *et al.*, 1995) onboard SOHO were used in this work.

TRACE images were obtained in the 1550 Å channel with a field of view (FOV) of  $\approx 384'' \times 384''$ , a pixel size of  $0.5'' \times 0.5''$ , and a cadence of 35 seconds. The Ca II H data from SOT were taken with a FOV of  $\approx 112'' \times 56''$ , a cadence of 30 seconds and a pixel size of  $0.11'' \times 0.11''$ . Description of the observations is summarized in Table 2. The data were reduced using the standard Solar Software package for the correction of missing pixels, cosmic-ray hits, CCD bias effects, and flat-field effects. All images from *Hinode* and TRACE were converted to SOHO’s view (L1). High-resolution photospheric line-of-sight magnetograms were obtained with MDI at a cadence of one minute with a pixel size of  $0.6'' \times 0.6''$  and a FOV of  $\approx 620'' \times 300''$ . All of the images were co-aligned with respect to TRACE. We used an available procedure for co-aligning TRACE with SOT and MDI data. When images from different instruments are compared, it is important to consider the difference in their spatial resolution. First we created an IDL map for all of the instruments; which is a structure that contains two-dimensional image data with accompanying pixel coordinate and spatial scale information. We used the routine *coreg\_map.pro* available in the SolarSoft library for resizing a map with respect to the other, by binning pixels, along with the routine *derot\_map.pro* to de-rotate one map with respect to the time of the other map for solar rotation compensation taking into account the roll angle of the satellite. These images were cross correlated and offset coordinates were obtained using the *get\_corel\_offset.pro* routine. These were then applied to SOT and MDI images. After the alignment, Figure 1 shows the location of the SOT FOV on the TRACE 1550 Å image. Contours on the image give the two polarities of the line-of-sight magnetic field obtained by MDI.

### 3. Data Analysis

For Fourier power and phase-difference analysis, we choose the longest overlap data between TRACE, and SOT (starting at 13:05:10 UT and ending at 15:29:41 UT). We had a few minutes data-gap before (12 minutes 29 seconds) and after (30 minutes 50 seconds) the selected SOT observations. During the selected time interval, 246 images were obtained in the TRACE 1550 Å passband with a cadence of 35 seconds, whereas 286 images were obtained with the Ca II H broadband filter (SOT) with a cadence of 30 seconds. Data-gaps of a few seconds were still present in the data which were linearly interpolated during the analysis. We should note that the selected time-series duration for the present quiet-Sun oscillation study is longer than any previous study and is suitable for the detection of oscillations having longer periodicities.

We extracted two sequences of sub-images from the TRACE data set, one having coverage of the MDI FOV (Figure 1) and another having coverage of the SOT FOV (Figure 2).

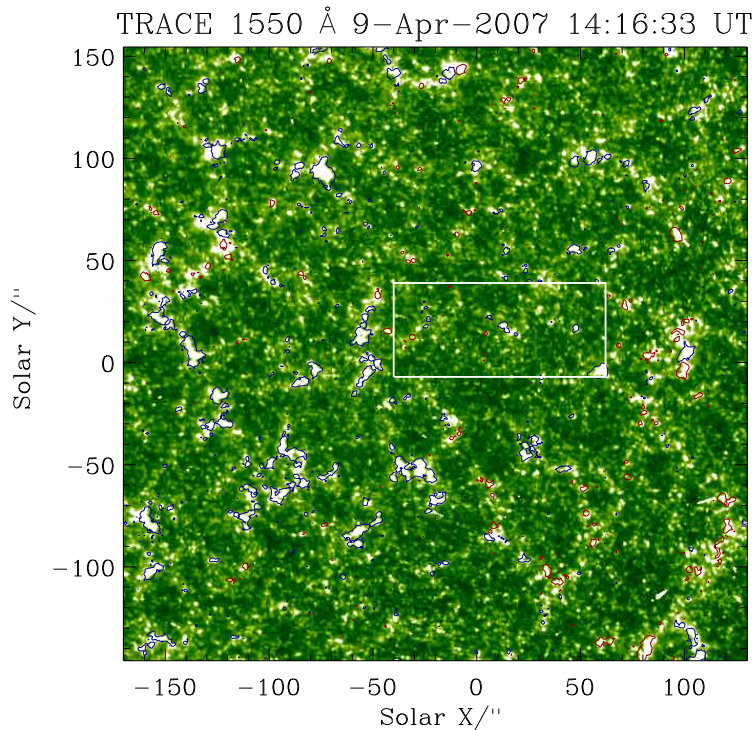


**Figure 1.** The quiet-Sun region observed with the TRACE 1550 Å passband on 9 April 2007. Contour levels show the line-of-sight magnetic field strength  $\geq |30|$  G obtained from the corresponding MDI image. SOT FOV is over-plotted as a rectangular box.

Figure 1 shows a TRACE image corresponding to the MDI FOV with the over-plotted MDI magnetic-field contours. Similarly, Figure 2 shows TRACE and SOT images with the SOT FOV over-plotted with magnetic-field contours, clearly illustrating the accuracy of the co-alignment between the TRACE and SOT data. High resolution movies of TRACE and MDI datasets, one corresponding to the MDI FOV and the other corresponding to the SOT FOV, are available as online material (*mdi\_tr\_full.mpeg* and *mdi\_tr\_small.mpeg* respectively). One can notice that the bright magnetic elements located in the network intensity-enhanced regions do not move much during the time interval of hours.

Figures 1 and 2 and the movies (see online) clearly show many bright magnetic (network) and dark non-magnetic (inter-network) regions. These distinguishable regions, gave us an opportunity to statistically compare the nature of the Fourier power and phase-differences simultaneously in both regions. We applied a Fourier analysis technique to both TRACE 1550 Å and SOT Ca II H images. A variation of the Fourier power with frequency were obtained for each spatial pixel. Four different frequency windows, 4.14–8.27 mHz (2–4 minutes, to see the 3 minutes period), 2.76–4.02 mHz (4–6 minutes, to see the 5 minutes period), 1.15–2.64 mHz (6–15 minutes, to see the intermediate periods), and up to 1.15 mHz (above 15 minutes, to see the longer periods), were chosen and the powers were then added together in these frequency ranges for producing power maps. A subset of these power maps can be found in Figure 3.

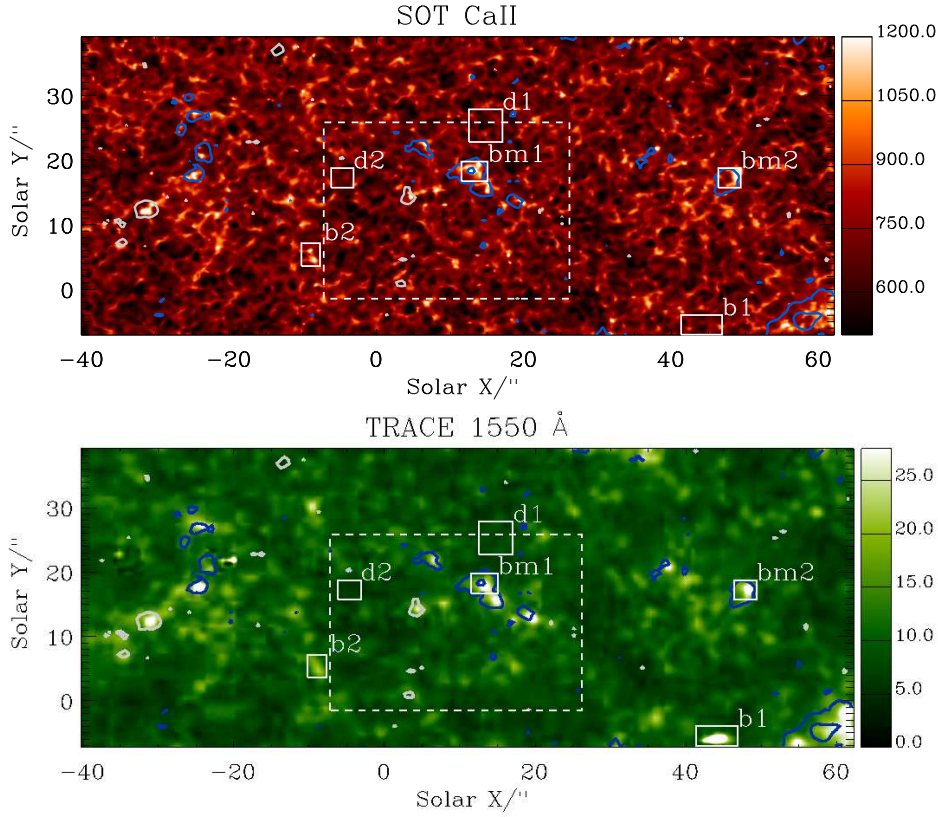


**Figure 2.** Ca II H (top) and TRACE 1550 Å (bottom) images over-plotted with the corresponding MDI magnetic field contours. Contour levels give the line-of-sight magnetic field strength of  $\geq |25|$  G. The continuous square boxes (bm1 and bm2), (b1 and b2) and (d1 and d2) correspond to bright magnetic, bright non-magnetic and dark non-magnetic regions, respectively whereas the dashed box gives the location of the power map as shown in Figure 3. The blue and white contours are the positive and negative polarities of the magnetic field.

In order to study the influence of the magnetic field on the oscillations, we classified three different regions namely, bright magnetic (bm), bright non-magnetic (b), and dark non-magnetic (d) regions (Figure 2). Bright magnetic regions correspond to TRACE 1550 Å enhanced intensity locations with a co-spatial magnetic field  $\geq \pm 25$  G as recorded by MDI. Similarly, bright non-magnetic regions correspond to TRACE 1550 Å bright locations without a co-spatial magnetic field  $\geq \pm 25$  G as recorded by MDI (e.g. b1 and b2). It is also possible that these bright regions were either associated with a co-spatial magnetic field  $\leq \pm 25$  G or had their footpoints in a region further away from them, *i.e.* not exactly underneath the bright locations, as structures on the Sun do not always expand radially. While the rest of the TRACE 1550 Å dark locations were described as dark non-magnetic regions (e.g. d1 and d2). Figure 6 shows the distribution of power with frequency corresponding to all three regions.

Now to focus our attention on a few bright magnetic network, bright non-magnetic locations and dark non-magnetic location, we fix one particular solar- $X$ , namely  $X \approx 14''$  and create a distance-time (XT) map from SOT Ca II H and the TRACE 1550 Å passbands (Figure 7). A wavelet analysis was performed on the representative bright (network) and

dark (inter–network) regions as identified in the TRACE 1550 Å XT map (see Figure 7). Wavelet results, corresponding to SOT Ca II H and TRACE 1550 Å, are shown in Figures 8 and 9. A phase difference analysis was performed between SOT Ca II H and TRACE 1550 Å passbands. The statistical analysis technique was used to calculate the time delay between the propagating waves from the Ca II layers to the layers of the TRACE 1550 Å. The corresponding phase delays are plotted in Figure 12 for the different regions. These are discussed in more detail in the next section.

## 4. Results and Discussion

### 4.1. Fourier Power Distribution in SOT Ca II H and TRACE 1550 Å Passbands

We will now discuss the Fourier power distribution in the SOT Ca II H and TRACE 1550 Å passband. In Figure 2, we show intensity images in the SOT Ca II H and TRACE 1550 Å passbands with the same FOV. To obtain the oscillatory power distribution, a standard Fourier power analysis technique was applied to each pixel. While applying this, the standard spatial resolution of each instrument was retained and the original signal was used without any trend subtractions or normalization to avoid any kind of bias in the analysis. The resultant Fourier power maps in the frequency ranges 4.14–8.27 mHz, 2.76–4.02 mHz, 1.15–2.64 mHz, and up to 1.15 mHz were obtained and a subset of these power maps can be found in Figure 3 for a region marked with dashed boxes in Figure 2.

*High frequency range:* the frequency range 4.14–8.27 mHz, which is centered at 3 minutes shows a lack of power in bright magnetic (network) regions as compared to the neighbouring dark non-magnetic (inter–network) regions. As network photospheric flux tubes expand with height (Gabriel, 1976), chromospheric oscillations that appear to be dominant in the inter–network can be suppressed above the photospheric network elements as reported by Judge, Tarbell, and Wilhelm (2001), Krijger *et al.* (2001), and recently by Vecchio *et al.* (2007) and Kontogiannis, Tsiropoula, and Tziotziou (2010) for the quiet–Sun regions, and by Tian and Xia (2008) at the boundary of an equatorial coronal–hole region.

*Intermediate frequency range:* the frequency range 2.76–4.02 mHz which is centered at 5 minutes shows improved power at some bright magnetic (network) regions as seen in the TRACE 1550 Å passband whereas there is still a lack of power in SOT Ca II H at many locations. The power in the bright regions is almost similar to the power in the high–frequency range. However, reduction in the power is observed in dark (inter–network) regions in the TRACE 1550 Å passbands as compared to the higher–frequency range. The observed power in both these ranges can be considered as a mixture of photospheric 5 minutes and chromospheric 3 minutes oscillations (Fossum and Carlsson, 2005).

The frequency range 1.15–2.64 mHz in the TRACE 1550 Å data also shows almost the same behaviour but, here, SOT Ca II H shows an enhancement in power in the bright magnetic (network) regions.

*Low frequency range:* the frequency range up to 1.15 mHz, which covers periods above 15 minutes, reveals a map which is completely dominated by a significant power at bright magnetic (network) regions in both the SOT Ca II H and the TRACE 1550 Å passbands. This scenario appears much cleaner when observed in the full TRACE 1550 Å FOV and is shown in Figure 4. The long–period powers are completely concentrated in network regions which give the impression of power halos and are similar to those seen by Vecchio *et al.* (2007), Tian and Xia (2008), and Kontogiannis, Tsiropoula, and Tziotziou (2010) for relatively shorter periods and at lower solar atmospheric heights. The above discussed observations

appear much cleaner for high- and intermediate-frequency ranges when seen in the TRACE full FOV in Figure 5.

The significant power at these low and intermediate frequencies can be explained with the inclined magnetic-field lines at the boundaries of network structure which provide “magnetoacoustic portals” through which low-frequency ( $<5$  mHz) magnetoacoustic waves can propagate into the solar chromosphere (Jefferies *et al.*, 2006). These waves might provide a significant source of energy for balancing the radiative losses of the ambient solar chromosphere.

Figure 6 shows the typical Fourier power corresponding to each spatial pixel within the specific regions (bm1, bm2, b1, b2, d1, and d2) marked as boxes in Figure 2, for both the SOT Ca II H (left panels) and TRACE 1550 Å (right panels) passbands. Here, we filtered out the low-frequency power with typically periods above 40 minutes which may arise due to the orbital effect of the spacecraft/instruments. From this figure, it is clear that low frequency oscillations completely dominate the power distribution in bright magnetic regions (top panels of Figure 6). Power at other frequencies mainly between 3–5 mHz begin to appear in comparison to low-frequency power in the bright non-magnetic regions (middle panels of Figure 6). Whereas power in both frequency ranges become comparable only in the dark non-magnetic regions. Thus this indicates that the low frequency power is present in all regions and high-frequency powers between 3 and 5 mHz are only comparable to them in dark non-magnetic regions (inter-network). These findings are different from the findings of Lites, Rutten, and Kalkofen (1993) who found low-frequency power only in network regions and high-frequency ( $\approx 5$  mHz) power in inter-network regions.

#### 4.2. Wavelet Analysis in Network and Inter-network Regions

In order to focus our attention on representative network and inter-network regions we first constructed a distance-time (XT) map for SOT images and TRACE 1550 Å images for a fixed solar- $X \approx 14''$ . Corresponding Fourier power distributions along the  $Y$ -direction are plotted next to the XT maps (see Figure 7). One can easily identify the network and the inter-network regions from the XT maps (see left panel of Figure 7). The representative network and inter-network regions were chosen at solar- $Y \approx 18''$  and  $\approx 25''$ , respectively for a wavelet analysis. Details on the wavelet analysis, which provides information on the temporal variation of the signal, are described by Torrence and Compo (1998). For the convolution with the time series in the wavelet transform, the Morlet function was chosen. The wavelet analysis was applied on the light curves obtained from SOT Ca II H, and TRACE 1550 Å for network and inter-network locations and are shown in Figures 8 and 9 where the top panels show the variation of the intensity with time. The light curves were obtained from the summed  $1'' \times 1''$  areas at the locations centered around the mentioned positions.

In the wavelet spectrum, the cross-hatched regions are locations where estimates of the oscillation period becomes unreliable and is called the cone-of-influence (COI). As a result of the COI, the maximum measurable period is shown by a horizontal dashed line in the global wavelet plots. The global wavelet plots are obtained by taking the mean over the wavelet time domain which is very similar to the Fourier transform as both are giving the distribution of power with respect to period or frequency. The periods at the locations of the first two maximum in the global wavelet spectrum are printed above the global wavelet spectrum.

Here also the original signal was chosen without any trend subtraction to perform the wavelet transform. As a result of this, the peak period falls within the COI and the confidence level of other periods outside the COI appears less. However, in all cases, clear

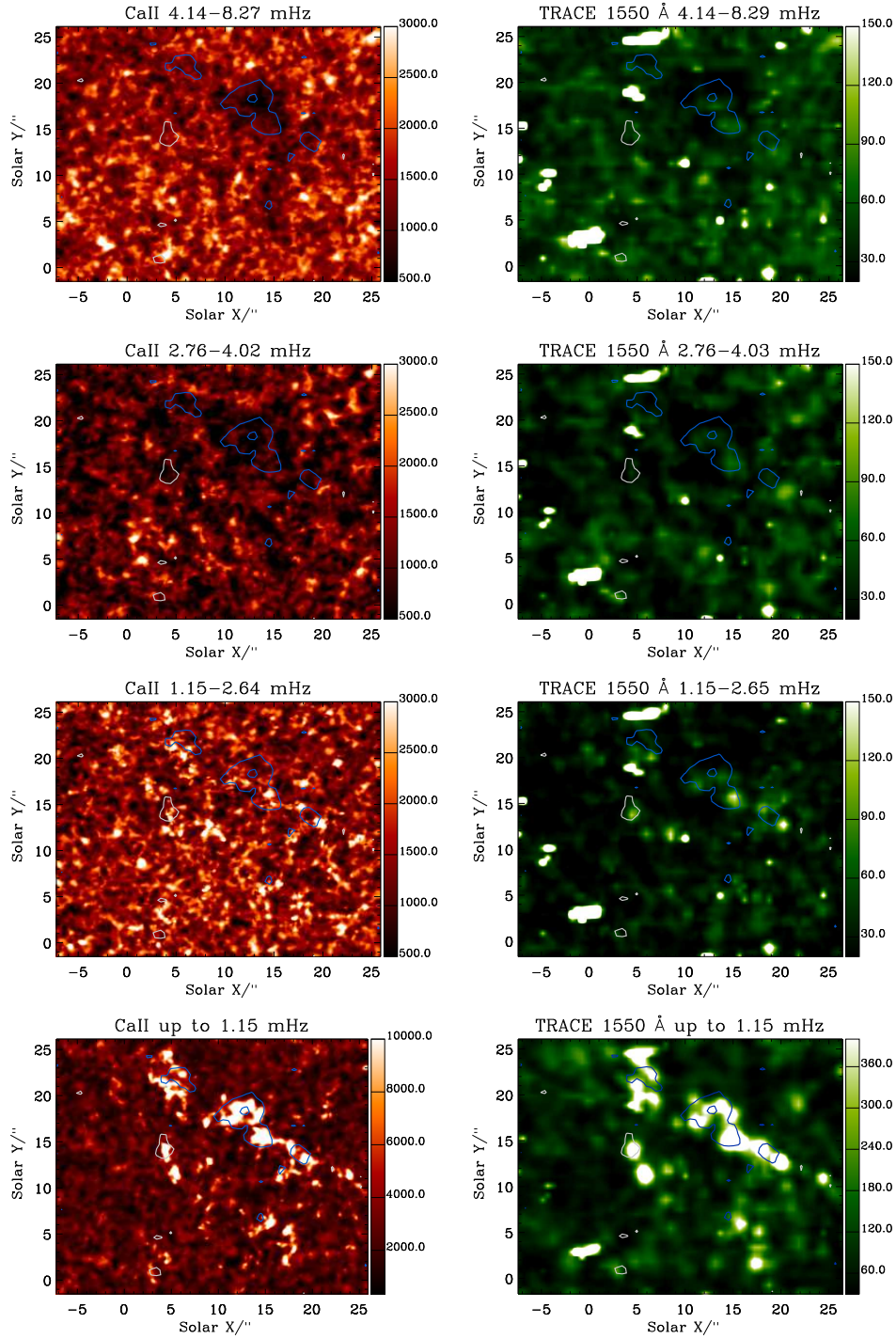


**Figure 3.** Oscillatory power map of Ca II H (left panels) and TRACE 1550 Å (right panels) on 9 April 2007 in different period ranges as labeled. Contour levels give the line-of-sight magnetic-field strength  $\geq |25|$  G measured from MDI. The blue and white contours are the positive and negative polarities of the magnetic field.



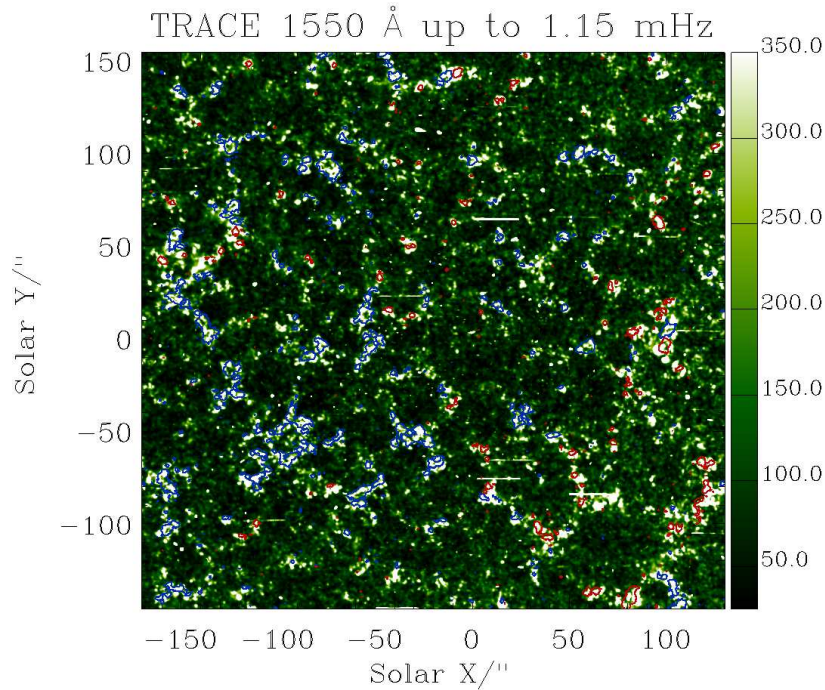


**Figure 4.** Oscillatory power in the period range 15 minutes and above for the full TRACE 1550 Å passband FOV on 9 April 2007. Contour levels give the line-of-sight magnetic-field strength  $\geq |30|$  G measured from MDI. The blue and red contours are the positive and negative polarities of the magnetic-field.

peaks of different periodicities are visible in all of the wavelet plots and these may become significant upon removal of periodicities lying within the COI. As mentioned earlier, we have divided the period ranges as a short period (2–6 minutes), an intermediate period (6–15 minutes) and a longer period (above 15 minutes). From the global wavelet spectrum, the corresponding period at the first dominant power peak is termed P1 whereas that at the second dominant power peak is termed P2. Based on the wavelet analysis plots and in particular on the global wavelet power distribution in Figures 8 and 9, we infer that most of the observed periods (P1 and P2) in the network region are in the longer period range from about 20 to 40 minutes. These are the periods which are dominating the power maps in the network regions in Figure 3. Whereas, the neighbouring inter-network region scenario is slightly different. Ca II H and TRACE 1550 Å show the dominant peak period of about 4 and 20 minutes, which are similar to the power seen in the dark regions of Figure 3. The longer period present near 45 minutes in Ca II H may be due to the *Hinode* orbit.

Lites, Rutten, and Kalkofen (1993) found that the long-period network oscillations in the chromosphere are not directly correlated with velocity fluctuations in the photosphere immediately underneath. Thus, they concluded that these disturbances are either confined to the chromosphere or are excited by photospheric events that take place at some horizontal distance from the point of observation. Spicules and their activities are closely related to the chromospheric network which extend upwards across the chromosphere reaching up to the height of the lower corona having typical life times of 5–15 minutes (Beckers, 1972;

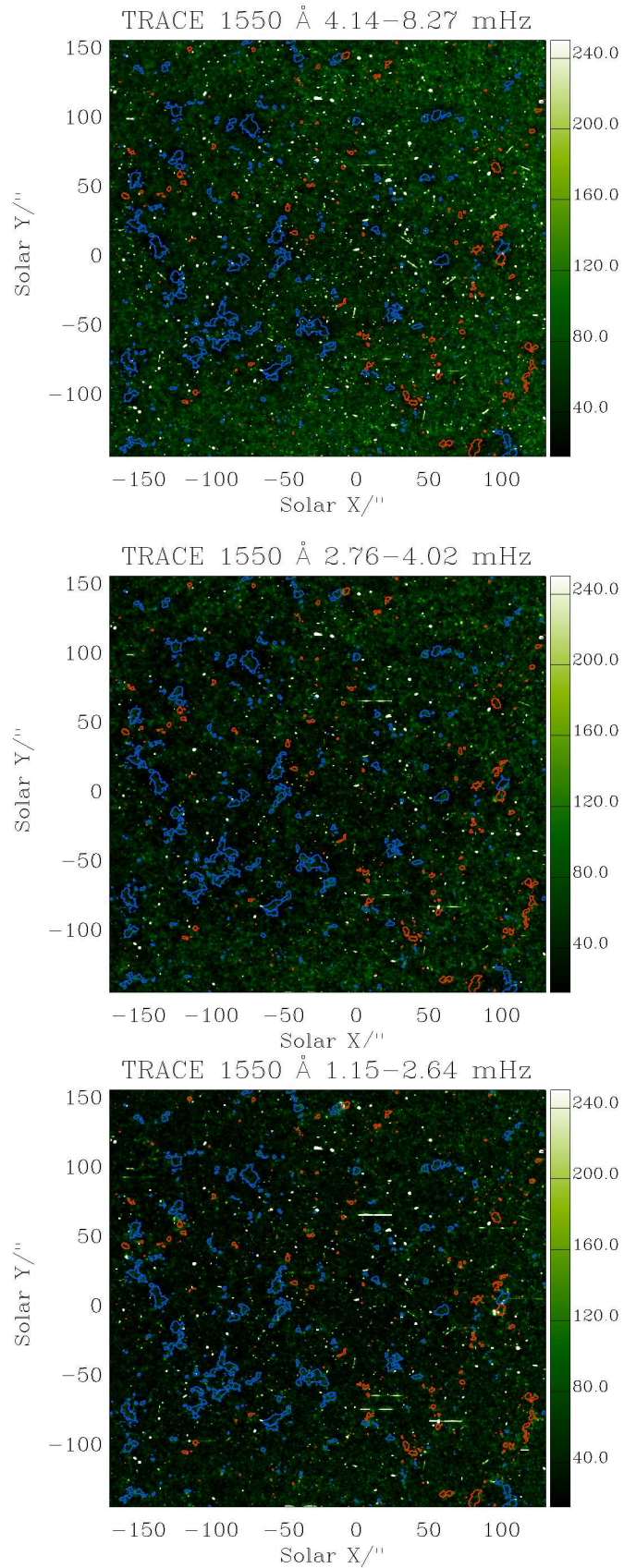


**Figure 5.** Oscillatory power map of TRACE 1550 Å on 9 April 2007 in different frequency ranges as labelled. Contour levels give the line-of-sight magnetic-field strength  $\geq 30$  G measured from MDI. The blue and red contours are the positive and negative polarities of the magnetic-field.

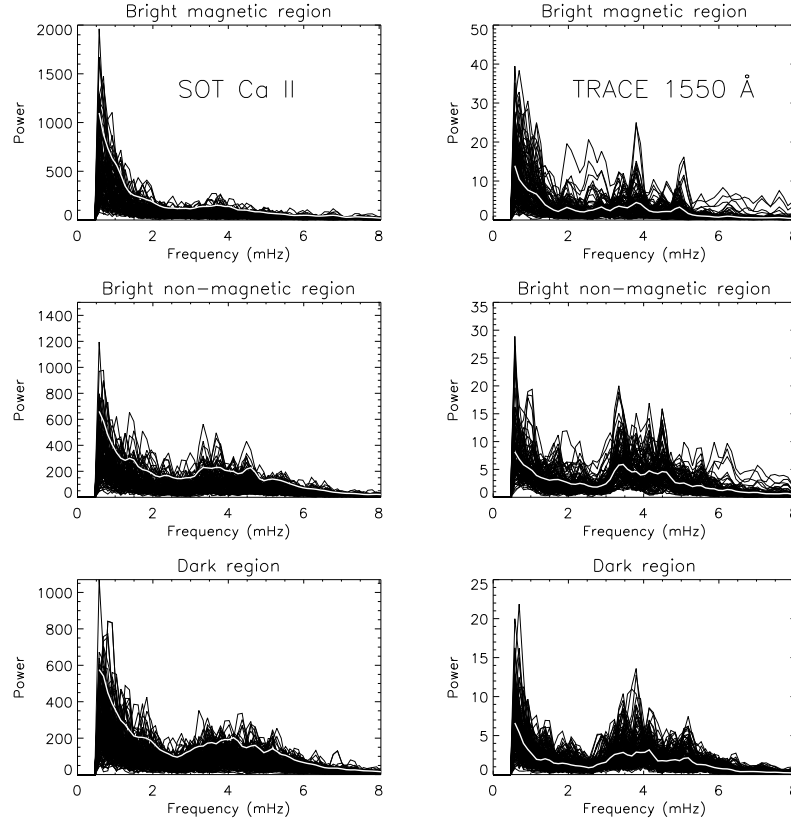


**Figure 6.** Fourier power distribution of Ca II H (left) and TRACE 1550 Å (right) for the few selected bright magnetic (bm1 and bm2), bright non-magnetic (b1 and b2) and dark non-magnetic (d1 and d2) regions as indicated in Figure 2. Overplotted white lines indicate the average Fourier power with respect to frequency.

Zaqarashvili and Erdélyi, 2009). Thus, these spicules could be responsible for driving these long-period network oscillations.

#### 4.3. Phase–Difference Analysis between SOT Ca II H and TRACE 1550 Å Passbands

As we see from the power maps in Figure 3 and oscillation periods from the wavelet plots, the Ca II H (chromosphere) and TRACE 1550 Å (low transition region/chromosphere) passbands show a similar kind of oscillation. Hence, it is most likely that the disturbances producing these oscillations could be due to waves propagating between the different temperature regions as covered by both passbands. To investigate whether this is actually the case, we measured the phase delays in intensity between the two passbands as a function of frequency for each of the measurable pixels in the image. The SOT Ca II H image array was rebinned to the spatial resolution of the TRACE instrument and the time series was linearly interpolated to obtain the same effective cadence as in the TRACE 1550 Å passband.

The phases were calculated from cross-power spectral estimates, following the techniques outlined in the appendix of Doyle *et al.* (1999). The errors in the phase were calculated based on Equation (A23) of Doyle *et al.* (1999). We averaged the phases in four

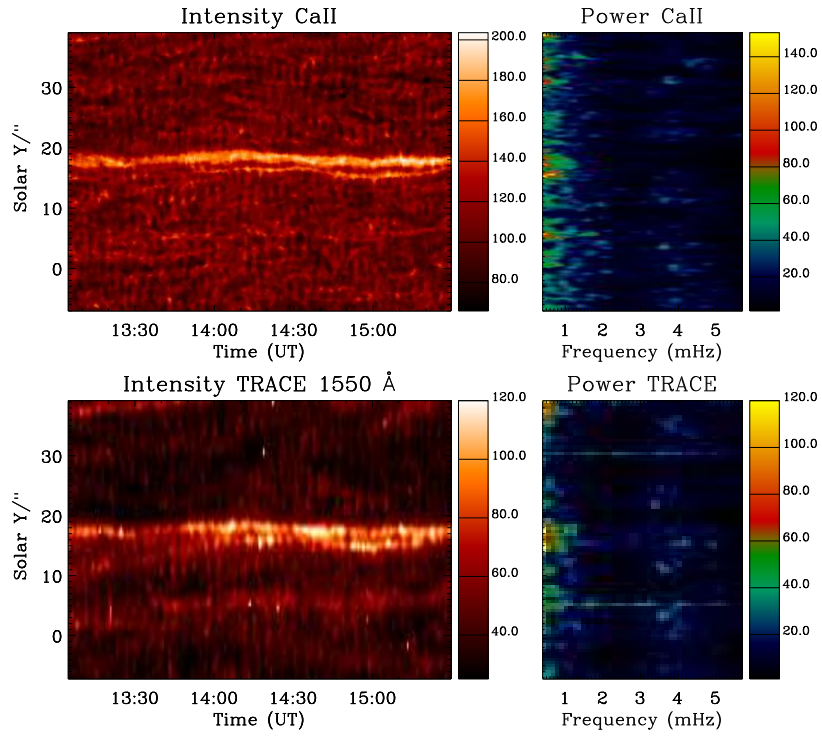


**Figure 7.** XT intensity map and respective Fourier power map of Ca II H (top) obtained from SOT BFG images and TRACE 1550 Å (bottom) images at solar- $X \approx 14''$ .

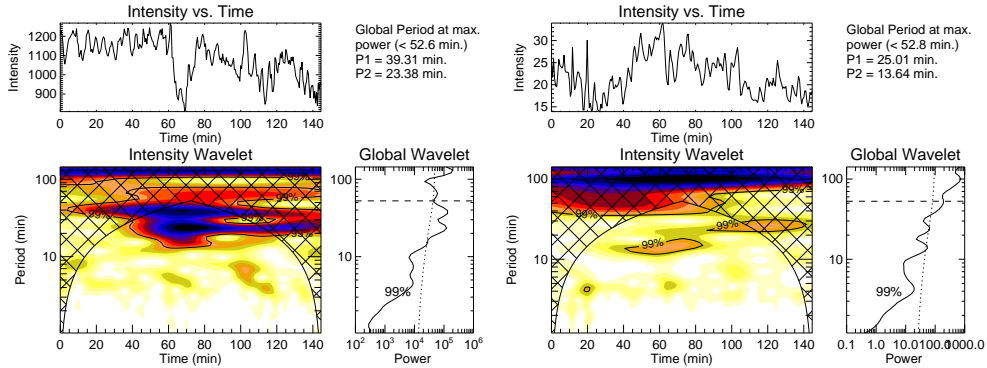


**Figure 8.** The wavelet results for the network location as identified from TRACE 1550 Å XT map at solar- $Y \approx 18''$  and solar- $X \approx 14''$  obtained from light curves of Ca II H (left) and TRACE 1550 Å (right). In each set, the top panels show the original light curve. The bottom left panels show the color-inverted wavelet power spectrum with 99 % confidence level contours while the bottom right panels show the global (averaged over time) wavelet power spectrum with 99 % global confidence level drawn. The periods P1 and P2 at the locations of the first two maxima in the global wavelet spectrum are printed above the global wavelet spectrum.

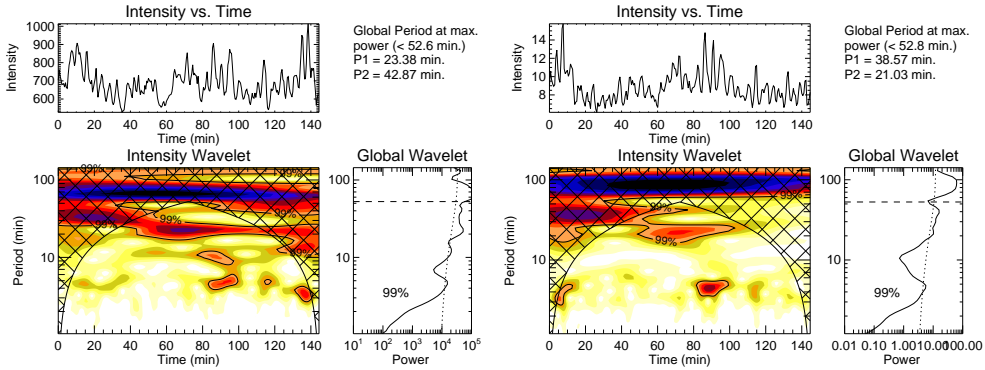


**Figure 9.** The wavelet results for the inter-network location as identified from TRACE 1550 Å XT map at solar- $Y \approx 25''$  and solar- $X \approx 14''$  obtained from the light curves of Ca II H (left) and TRACE 1550 Å (right). In each set, the top panels show the original light curve. The bottom left panels show the color-inverted wavelet power spectrum with 99 % confidence level contours while the bottom right panels show the global (averaged over time) wavelet power spectrum with 99% global confidence level drawn. The periods P1 and P2 at the locations of the first two maxima in the global wavelet spectrum are printed above the global wavelet spectrum.

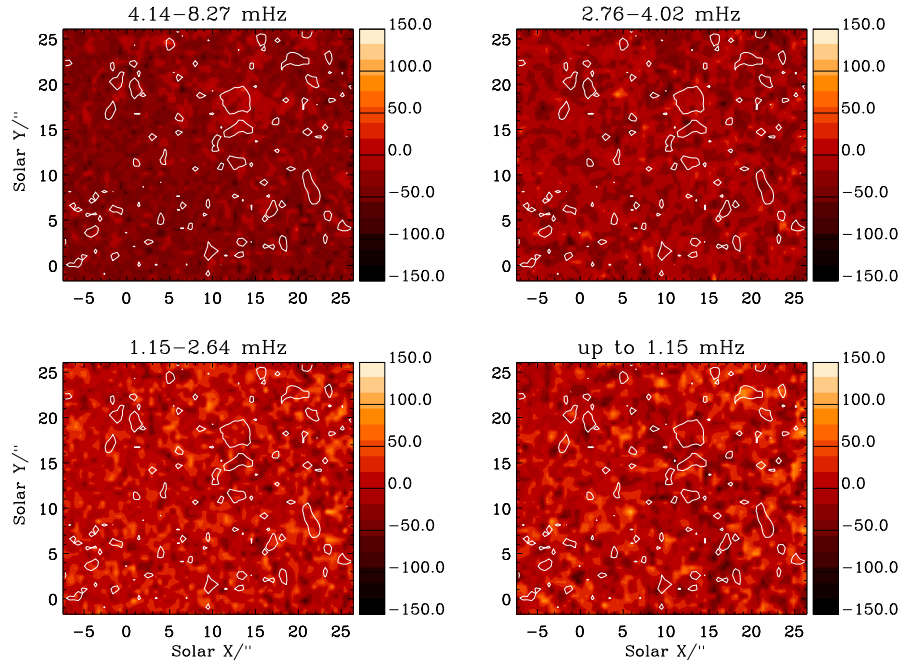


**Figure 10.** Phase-difference maps obtained between Ca II H and TRACE 1550 Å on 9 April 2007 in different frequency bands as indicated on the plot. Contour levels give the Ca II H intensity. Color scales are in degrees.

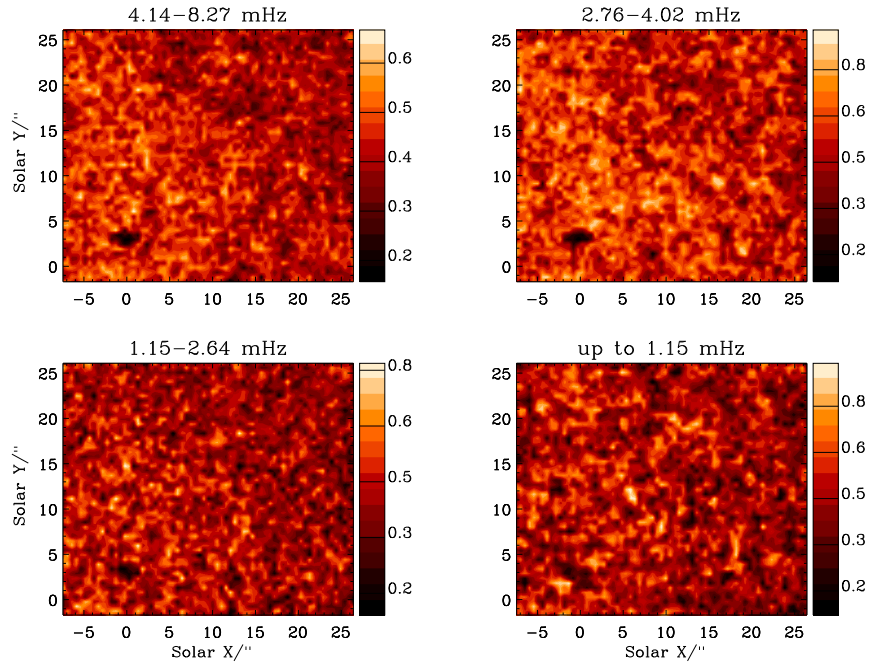


**Figure 11.** Coherency maps obtained between Ca II H and TRACE 1550 Å on 9 April 2007 in different frequency bands corresponding to phase-difference maps in Figure 10.

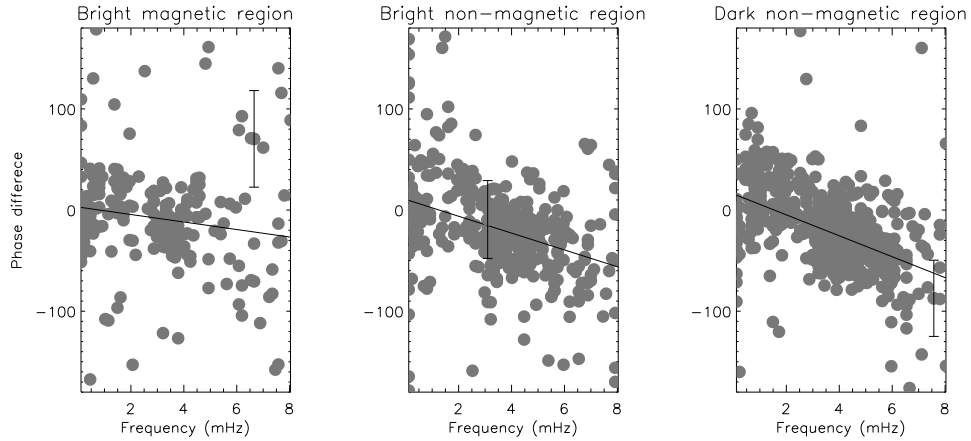


**Figure 12.** Phase-distribution of Ca II H and TRACE 1550 Å for the selected bright magnetic, bright non-magnetic, and dark non-magnetic regions and time delays are  $-(10.3 \pm 3.8)$  seconds,  $-(23.1 \pm 2.9)$  seconds, and  $-(28.7 \pm 3.0)$  seconds respectively.

bands and assigned an average phase difference to each pixel in each band. The resultant phase-difference maps in the four frequency bands are shown in Figure 10 with the corresponding coherency maps shown in Figure 11. In the phase-difference maps, the brighter pixels (corresponding to positive phases) represent downward-propagating waves, whereas darker pixels (corresponding to negative phases) are representative of upward-propagating waves. Figure 10 clearly shows that the phase map for the high frequency band is globally darker in nature when compared to the phase maps of other lower frequency bands. The phase map of the lowest frequency band (up to 1.15 mHz with periods 15 minutes and above) appears to be the brightest as compared to the other frequency ranges globally. This indicates the frequency dependent nature of the phase-distributions.

For high-frequency bands, the phases are more negative in nature (average phase-difference is about  $-15^\circ$ ) whereas for low-frequency bands, the phases are positive and near to  $0^\circ$  (average phase-difference is about  $4^\circ$ ). In Section 4.1, we pointed out that the low-frequencies powers are mainly concentrated in network regions, whereas inter-network regions have both low- and high- frequency powers. Hence, we interpret the negative phases in the high-frequency bands as due to upward-propagating waves in the inter-network regions, whereas the near-zero positive phases in low-frequency bands could be caused by the evanescent nature of waves present in both the network and the inter-network regions. Also when each map is observed very closely, small mesh-like structures are visible all over, which indicates that the upward and downward propagation occurs in the neighbourhood, but it is difficult to identify the preferred locations of these meshes either in the network or in the inter-network regions.

By measuring phase delays between intensity and velocity oscillations of different line pairs, O'Shea, Banerjee, and Doyle (2007) showed that propagating slow magnetoacoustic waves are present in coronal holes, and that they occur preferentially in bright regions that are associated with magnetic-field concentrations in the form of loops or bright points. In this section, following a similar analysis we will try to find out if there are fixed time delays between the Ca II H (chromosphere) and TRACE 1550 Å (low transition region/chromosphere). For a specific location, the phase-difference as a function of frequency is governed by the equation (Athay and White, 1979):

$$\Delta\phi = 2\pi fT, \quad (1)$$

where  $f$  is the frequency and  $T$  the time delay in seconds. The phase-difference will vary linearly with  $f$ , and will change by  $360^\circ$  over frequency intervals of  $\Delta f = 1/T$ . This will give rise to parallel lines in  $\Delta\phi$  vs.  $f$  plots at fixed frequency intervals ( $\Delta f = 1/T$ ), corresponding to a fixed time delay  $T$ . Hence, it is possible to measure the time delay of wave propagation between two heights in the atmosphere for a specific location (O'Shea, Banerjee, and Doyle, 2006, 2007; Gupta *et al.*, 2009). To obtain the time delay corresponding to different regions identified *viz.*, bright magnetic, bright non-magnetic and dark non-magnetic as marked in Figure 2, phase distribution plots obtained from the Ca II H and TRACE 1550 Å passbands were produced for these regions. We choose only those phases (corresponding to each spatial pixel) where the squared coherencies are greater than a significance of 95.4% ( $2\sigma$ ) for further analysis. The calculated phase delays were plotted over the full  $-180^\circ$  to  $+180^\circ$  ( $360^\circ$ ) range and as a function of the measured oscillation frequency for all three regions (see Figure 12). As expected, the phases were lined up along an inclined line as predicted by the phase equation (Equation 1) for all three regions. A straight line was fitted by taking into account all phase points. From the slope of this straight line, the measured time delays are  $-(10.3 \pm 3.8)$  seconds,  $-(23.1 \pm 2.9)$  seconds, and  $-(28.7 \pm 3.0)$  seconds for bright magnetic,

bright non-magnetic, and dark non-magnetic regions respectively. A negative time delay indicates upward propagation of waves. In this case, the measured time delays are very small, therefore the fixed frequency intervals ( $\Delta f = 1/T$ ) for the parallel lines are very large, and, hence, only one line is visible in the plot as compared to the many parallel lines in previous studies (O’Shea, Banerjee, and Doyle, 2006, 2007; Gupta *et al.*, 2009). Furthermore, the slope of the fitted line is determined mostly by the high frequency phase difference data points, whose distance from the zero-degree line are greater than those of low-frequency phase-difference data points. In the third panel of Figure 12 (dark non-magnetic regions), based on the scatter of the data points at the low-frequency range, up to 3 mHz, phases may be considered to be distributed around  $0^\circ$ . This is an indication of evanescent low-frequency waves. At the bright magnetic regions (first panel of Figure 12), there are data points at large phase-differences which indicate high coherency at low-frequency, and could be interpreted as low-frequency waves. The measured small delays between these two passbands indicate that these two covered regions are formed very close in the atmosphere. Results from this analysis also indicate that the wave speed is smaller in non-magnetic regions as compared to magnetic regions.

## 5. Summary and Conclusion

Quiet-Sun oscillations were studied using the Fourier power and phase-difference analysis from the intensity time series observed simultaneously in SOT Ca II H and TRACE 1550 Å. Fourier power maps reveal that, 3 and 5 minutes power are suppressed around the bright magnetic-network regions at chromospheric heights. This suggests the existence of “magnetic shadows” as seen recently by Vecchio *et al.* (2007), Tian and Xia (2008), and Kontogiannis, Tsiropoula, and Tziotziou (2010), whereas above the 15 minutes period range we see very high-power above the magnetic network, which forms power halo like structure. Wavelet analysis reveals the presence of 15–30 minutes periodicities at chromospheric and transition-region heights (corresponding to network regions). We can only speculate on the nature of these low-frequency oscillations. They appear to be of slow magnetoacoustic in nature. They can be either propagating type (more pronounced in the network locations) or standing type (corresponding to the inter-network regions with low-lying magnetic loops).

This scenario is consistent with the phase analysis results as well, where we see the presence of pronounced upward propagation corresponding to magnetic-network regions and a mixture of upward and downward propagations at other locations. Mariska and Muglach (2010) have also reported the presence of both standing and propagating waves with many periods longer than 10 minutes. They also state that a clear picture of all the wave modes that might be associated with active regions has not yet emerged. They further speculate that the periods of the waves are related to impulsive heating which may be producing them.

Earlier work by Doyle *et al.* (1999) indicated excess power at very low frequencies (based on SUMER C II data), however, since these were sit-and-stare observations without rotational compensations, the implications are that this power comes from structures larger than  $1''$ . Most earlier works were affected by the same limitation, either having a shorter time series or not having rotational compensation.

Short period oscillations are dominant in the dark non-magnetic regions. Time-delay analysis performed on phase-differences measured between SOT Ca II H and TRACE 1550 Å passbands indicates different time delays corresponding to magnetic and non-magnetic regions. As explained by Jefferies *et al.* (2006), the low-frequency photospheric oscillations can propagate into the solar chromosphere through “magnetoacoustic portals”. They have



also pointed out that a sizable fraction of the photospheric acoustic power at frequencies below the cut-off might propagate to higher layers within and around the quiet magnetic network elements. In a similar way, these long period waves ( $> 5$  minutes) can propagate up to coronal heights through inclined magnetic-field lines, which could reduce the cut-off frequency (De Pontieu, Erdélyi, and James, 2004). Vecchio *et al.* (2007) showed that waves with frequencies less than the acoustic cut-off frequency around magnetic-network structures can propagate through inclined magnetic fields in the form of fibril-like structures. Spicules and their activities are closely related to the chromospheric network and fibrils which extend upwards across the chromosphere reaching up to the height of the lower corona. Thus, these spicules could be responsible for driving the long-period network oscillations. Using SOT data, Lawrence and Cadavid (2010) showed similar space-time distributions of intensity fluctuations from 2–3 hours sequences. In the frequency range  $5.5 < f < 8.0$  mHz, both the G-band and Ca II H-line oscillations show suppression in the presence of magnetic fields. They also found that oscillatory powers at these frequencies and at lower frequencies, lie in a mesh pattern with a cell scale of 2–3 Mm, clearly larger than normal granulation, and with correlation times on the order of hours. In our analysis of combined *Hinode* and TRACE capabilities we find a very similar pattern.

In open-field regions, longer periods of 10–15 minutes have been detected along polar plumes (DeForest and Gurman, 1998; Banerjee, O’Shea, and Doyle, 2000; Banerjee *et al.*, 2009), and were interpreted as compressive waves by Ofman, Nakariakov, and DeForest (1999), 15–20 minutes period waves along interplume regions observed by Gupta *et al.* (2010) were explained as Alfvénic or fast mode waves. Banerjee *et al.* (2001) observed 2–4 mHz network oscillations in the low chromospheric and transition-region lines in both intensity and velocity, which were interpreted in terms of kink and sausage waves propagating upwards along thin magnetic flux tubes. Here, intensity oscillations may result from the presence of magnetoacoustic waves which could provide significant energy to heat the solar atmosphere.

There are a number of studies involving G-band (photospheric) and Ca II H (chromospheric) image sequences from the *Dutch Open Telescope* (DOT) (Rutten, de Wijn, and Sütterlin, 2004; de Wijn *et al.*, 2005). Similar studies were made for different TRACE passbands also (De Wijn, Rutten, and Tarbell, 2005) but to our knowledge this is the first simultaneous study between SOT Ca II H and TRACE 1550 Å passband.

To extend this work we need spectral imaging data to identify the wave mode. This requires acquisition of long-duration spectral and imaging data which may be obtained from future observations such as EIS and SOT onboard *Hinode*, and AIA and HMI onboard SDO. In order to establish whether these waves are transverse or longitudinal to the magnetic field, observations of magnetic oscillations at varying limb distances are needed to measure the significant horizontal components of these motions.

**Acknowledgements** We thank the referee for their careful reading and valuable suggestions which has enabled us to improve the manuscript substantially. Research at Armagh Observatory is grant-aided by the N. Ireland Dept. of Culture, Arts and Leisure. We thank STFC for support via ST/J001082/1. The *Transition Region and Coronal Explorer* (TRACE), is a mission of the Stanford–Lockheed Institute for Space Research, and part of the NASA Small Explorer program. *Hinode* is a Japanese mission developed and launched by ISAS/JAXA, with NAOJ as domestic partner and NASA and STFC (UK) as international partners. It is operated by these agencies in co-operation with ESA and NSC (Norway).

## References

- Athay, R.G., White, O.R.: 1979, Chromospheric oscillations observed with OSO 8. IV - Power and phase spectra for C IV. *Astrophys. J.* **229**, 1147–1162. doi:10.1086/157050.
- Banerjee, D., O’Shea, E., Doyle, J.G.: 2000, Long-Period Oscillations in Polar Plumes as Observed by cds on Soho. *Solar Phys.* **196**, 63–78.
- Banerjee, D., O’Shea, E., Doyle, J.G., Goossens, M.: 2001, The nature of network oscillations. *Astron. Astrophys.* **371**, 1137–1149. doi:10.1051/0004-6361:20010426.
- Banerjee, D., Teriaca, L., Gupta, G.R., Imada, S., Stenborg, G., Solanki, S.K.: 2009, Propagating waves in polar coronal holes as seen by SUMER and EIS. *Astron. Astrophys.* **499**, L29–L32. doi:10.1051/0004-6361/200912059.
- Beckers, J.M.: 1972, Solar Spicules. *Ann. Rev. Astron. Astrophys.* **10**, 73–100. doi:10.1146/annurev.aa.10.090172.000445.
- Carlsson, M., Judge, P.G., Wilhelm, K.: 1997, SUMER Observations Confirm the Dynamic Nature of the Quiet Solar Outer Atmosphere: The Internetwork Chromosphere. *Astrophys. J. Lett.* **486**, L63. doi:10.1086/310836.
- Dame, L., Gouttebroze, P., Malherbe, J.: 1984, Observation and analysis of intensity oscillations in the solar K-line. *Astron. Astrophys.* **130**, 331–340.
- De Pontieu, B., Erdélyi, R., James, S.P.: 2004, Solar chromospheric spicules from the leakage of photospheric oscillations and flows. *Nature* **430**, 536–539. doi:10.1038/nature02749.
- de Wijn, A.G., Rutten, R.J., Haverkamp, E.M.W.P., Sütterlin, P.: 2005, DOT tomography of the solar atmosphere. IV. Magnetic patches in internetwork areas. *Astron. Astrophys.* **441**, 1183–1190. doi:10.1051/0004-6361:20053373.
- De Wijn, A.G., Rutten, R.J., Tarbell, T.D.: 2005, Dynamics of the solar chromosphere. V. High-frequency modulation in ultraviolet image sequences from TRACE. *Astron. Astrophys.* **430**, 1119–1127. doi:10.1051/0004-6361:20041727.
- DeForest, C.E., Gurman, J.B.: 1998, Observation of Quasi-periodic Compressive Waves in Solar Polar Plumes. *Astrophys. J. Lett.* **501**, L217. doi:10.1086/311460.
- Doyle, J.G., van den Oord, G.H.J., O’Shea, E., Banerjee, D.: 1999, Exploring the dynamical nature of the lower solar chromosphere. *Astron. Astrophys.* **347**, 335–347.
- Fossum, A., Carlsson, M.: 2005, High-frequency acoustic waves are not sufficient to heat the solar chromosphere. *Nature* **435**, 919–921. doi:10.1038/nature03695.
- Gabriel, A.H.: 1976, A magnetic model of the solar transition region. *Roy. Soc. London Phil. Trans. Ser. A* **281**, 339–352.
- Gupta, G.R., Banerjee, D., Teriaca, L., Imada, S., Solanki, S.: 2010, Accelerating Waves in Polar Coronal Holes as Seen by EIS and SUMER. *Astrophys. J.* **718**, 11–22. doi:10.1088/0004-637X/718/1/11.
- Gupta, G.R., O’Shea, E., Banerjee, D., Popescu, M., Doyle, J.G.: 2009, On the statistical detection of propagating waves in polar coronal holes. *Astron. Astrophys.* **493**, 251–257. doi:10.1051/0004-6361:200810602.
- Hale, G.E., Ellerman, F.: 1904, Calcium and Hydrogen Flocculi. *Astrophys. J.* **19**, 41–52. doi:10.1086/141083.
- Handy, B.N., Acton, L.W., Kankelborg, C.C., Wolfson, C.J., Akin, D.J., Bruner, M.E., Carvalho, R., Catura, R.C., Chevalier, R., Duncan, D.W., Edwards, C.G., Feinstein, C.N., Freeland, S.L., Friedlaender, F.M., Hoffmann, C.H., Hurlburt, N.E., Jurcevich, B.K., Katz, N.L., Kelly, G.A., Lemen, J.R., Levay, M., Lindgren, R.W., Mathur, D.P., Meyer, S.B., Morrison, S.J., Morrison, M.D., Nightingale, R.W., Pope, T.P., Rehse, R.A., Schrijver, C.J., Shine, R.A., Shing, L., Strong, K.T., Tarbell, T.D., Title, A.M., Torgerson, D.D., Golub, L., Bookbinder, J.A., Caldwell, D., Cheimets, P.N., Davis, W.N., Deluca, E.E., McMullen, R.A., Warren, H.P., Amato, D., Fisher, R., Maldonado, H., Parkinson, C.: 1999, The transition region and coronal explorer. *Solar Phys.* **187**, 229–260. doi:10.1023/A:1005166902804.
- Hasan, S.S.: 2008, Chromospheric dynamics. *Adv. Space Res.* **42**, 86–95. doi:10.1016/j.asr.2007.08.019.
- Jefferies, S.M., McIntosh, S.W., Armstrong, J.D., Bogdan, T.J., Cacciani, A., Fleck, B.: 2006, Magnetoacoustic Portals and the Basal Heating of the Solar Chromosphere. *Astrophys. J. Lett.* **648**, L151–L155. doi:10.1086/508165.
- Judge, P.G., Tarbell, T.D., Wilhelm, K.: 2001, A Study of Chromospheric Oscillations Using the SOHO and TRACE Spacecraft. *Astrophys. J.* **554**, 424–444. doi:10.1086/321383.
- Kontogiannis, I., Tsiropoula, G., Tziotziou, K.: 2010, Power halo and magnetic shadow in a solar quiet region observed in the H $\alpha$  line. *Astron. Astrophys.* **510**, A41. doi:10.1051/0004-6361/200912841.
- Krijger, J.M., Rutten, R.J., Lites, B.W., Straus, T., Shine, R.A., Tarbell, T.D.: 2001, Dynamics of the solar chromosphere. III. Ultraviolet brightness oscillations from TRACE. *Astron. Astrophys.* **379**, 1052–1082. doi:10.1051/0004-6361:20011320.

- Lawrence, J.K., Cadavid, A.C.: 2010, Space - Time Distribution of G-band and Ca ii H-line Intensity Oscillations in Hinode/SOT - FG Observations. *Solar Phys.* **261**, 35 – 52. doi:10.1007/s11207-009-9481-z.
- Lites, B.W., Rutten, R.J., Kalkofen, W.: 1993, Dynamics of the solar chromosphere. I - Long-period network oscillations. *Astrophys. J.* **414**, 345 – 356. doi:10.1086/173081.
- Mariska, J.T., Muglach, K.: 2010, Doppler-shift, Intensity, and Density Oscillations Observed with the Extreme Ultraviolet Imaging Spectrometer on Hinode. *Astrophys. J.* **713**, 573 – 583. doi:10.1088/0004-637X/713/1/573.
- McIntosh, S.W., Judge, P.G.: 2001, On the Nature of Magnetic Shadows in the Solar Chromosphere. *Astrophys. J.* **561**, 420 – 426. doi:10.1086/323068.
- Ofman, L., Nakariakov, V.M., DeForest, C.E.: 1999, Slow Magnetosonic Waves in Coronal Plumes. *Astrophys. J.* **514**, 441 – 447. doi:10.1086/306944.
- O’Shea, E., Banerjee, D., Doyle, J.G.: 2006, Magnetoacoustic wave propagation in off-limb polar regions. *Astron. Astrophys.* **452**, 1059 – 1068. doi:10.1051/0004-6361:20053687.
- O’Shea, E., Banerjee, D., Doyle, J.G.: 2007, A statistical study of wave propagation in coronal holes. *Astron. Astrophys.* **463**, 713 – 725. doi:10.1051/0004-6361:20065592.
- Rutten, R.J., de Wijn, A.G., Sütterlin, P.: 2004, DOT tomography of the solar atmosphere. II. Reversed granulation in Ca II H. *Astron. Astrophys.* **416**, 333 – 340. doi:10.1051/0004-6361:20035636.
- Scherrer, P.H., Bogart, R.S., Bush, R.I., Hoeksema, J.T., Kosovichev, A.G., Schou, J., Rosenberg, W., Springer, L., Tarbell, T.D., Title, A., Wolfson, C.J., Zayer, I., MDI Engineering Team, : 1995, The Solar Oscillations Investigation - Michelson Doppler Imager. *Solar Phys.* **162**, 129 – 188. doi:10.1007/BF00733429.
- Simon, G.W., Leighton, R.B.: 1964, Velocity Fields in the Solar Atmosphere. III. Large-Scale Motions, the Chromospheric Network, and Magnetic Fields. *Astrophys. J.* **140**, 1120 – 1147. doi:10.1086/148010.
- Skumanich, A., Smythe, C., Frazier, E.N.: 1975, On the statistical description of inhomogeneities in the quiet solar atmosphere. I - Linear regression analysis and absolute calibration of multichannel observations of the Ca+/ emission network. *Astrophys. J.* **200**, 747 – 764. doi:10.1086/153846.
- Tian, H., Xia, L.: 2008, Network oscillations at the boundary of an equatorial coronal hole. *Astron. Astrophys.* **488**, 331 – 337. doi:10.1051/0004-6361:200810124.
- Torrence, C., Compo, G.P.: 1998, A Practical Guide to Wavelet Analysis. *Bull. Am. Meteorol. Soc.* **79**, 61 – 78. doi:10.1175/1520-0477(1998)079<0061:APGTWA>2.0.CO;2.
- Tsuneta, S., Ichimoto, K., Katsukawa, Y., Nagata, S., Otsubo, M., Shimizu, T., Suematsu, Y., Nakagiri, M., Noguchi, M., Tarbell, T., Title, A., Shine, R., Rosenberg, W., Hoffmann, C., Jurcevich, B., Kushner, G., Levay, M., Lites, B., Elmore, D., Matsushita, T., Kawaguchi, N., Saito, H., Mikami, I., Hill, L.D., Owens, J.K.: 2008, The Solar Optical Telescope for the Hinode Mission: An Overview. *Solar Phys.* **249**, 167 – 196. doi:10.1007/s11207-008-9174-z.
- Vecchio, A., Cauzzi, G., Reardon, K.P., Janssen, K., Rimmele, T.: 2007, Solar atmospheric oscillations and the chromospheric magnetic topology. *Astron. Astrophys.* **461**, L1 – L4. doi:10.1051/0004-6361:20066415.
- Wikstøl, Ø., Hansteen, V.H., Carlsson, M., Judge, P.G.: 2000, Chromospheric and Transition Region Internetwork Oscillations: A Signature of Upward-propagating Waves. *Astrophys. J.* **531**, 1150 – 1160. doi:10.1086/308475.
- Zaqarashvili, T.V., Erdélyi, R.: 2009, Oscillations and Waves in Solar Spicules. *Space Sci. Rev.* **149**, 355 – 388. doi:10.1007/s11214-009-9549-y.

